Performance analysis of anomalous photocatalytic activity of Cr-doped TiO$_2$ nanoparticles [Cr$_{(x)}$TiO$_{2(1-x)}$]

Jyoti Bansal[1,2] · Rana Tabassum[1] · Sanjay Kumar Swami[2] · Swati Bishnoi[2] · Pargam Vashishtha[2] · Govind Gupta[2] · S. N. Sharma[2] · A. K. Hafiz[1]

Abstract

We report the synthesis and characterisation of pristine and chromium (Cr) metal ion-doped titanium dioxide nanoparticles [Cr$_{(x)}$TiO$_{2(1-x)}$] to study the anomalous effect of Cr doping on the photocatalytic property of TiO$_2$. The presence of dopants generates more number of recombination pairs and increases surface coverage sites which decreases photocatalytic activity. We study the structural morphology of the synthesised Cr$_{(x)}$TiO$_{2(1-x)}$ samples using X-ray diffraction (XRD) and X-ray photoelectron spectroscopy analysis. The effect of Cr^{3+} ions on the optical properties of TiO$_2$ has been studied using various imaging and spectroscopic techniques. Further, the effect of doping of Cr on the photocatalytic activity of TiO$_2$ has been analysed in detail. The concentration of Cr in TiO$_2$ has been chosen as 0, 1, 5 and 10% by weight. It has been observed that the pristine TiO$_2$ exhibits better photocatalytic activity as compared to Cr-doped TiO$_2$ irrespective of the Cr concentration. This can be attributed to the fact that due to Cr doping in TiO$_2$, the number of available adsorption sites for malachite green reduces which degrades its photocatalytic activity. It is also confirmed by photoluminescence (PL) and time-resolved photoluminescence spectroscopy. PL intensity increases, and lifetime decreases with increase in doping concentration. Radiative recombination of electron and hole pairs of Cr^{3+} in TiO$_2$ degrades its photocatalytic activity. The degradation efficiency is found to be 96% in the case of pristine TiO$_2$ which reduces to 12% when doped with $x = 10\%$ concentration of chromium. Therefore, it is observed that in comparison with Cr-doped TiO$_2$, pristine TiO$_2$ exhibits an improved photocatalytic activity which shows the anomalous effect of Cr doping on the photocatalytic property of TiO$_2$.

Keywords TiO$_2$ · Cr$_{(x)}$TiO$_{2(1-x)}$ · Malachite green dye (MG) · Nanoparticles and photocatalysis

1 Introduction

The fabrication and characterisation of nanomaterials have been carried out for different fields such as chemical, biological and biochemical sensing which includes photocatalysis [1], photovoltaics [2], sensors, LED, etc. [3–8]. In recent years, there has been a renewed interest in research related to TiO$_2$ owing to its characteristic properties such as efficient charge transfer [7], electrical conductivity, chemical

✉ S. N. Sharma
shailesh@nplindia.org

✉ A. K. Hafiz
ahafiz@jmi.ac.in

1 Centre for Nanoscience and Nanotechnology, Jamia Millia Islamia, New Delhi 110025, India

2 CSIR-National Physical Laboratory, Dr K.S. Krishnan Marg, New Delhi 110012, India

stability and cost-effectiveness. In spite of all these properties of TiO$_2$, some properties such as wide band gap, fast charge recombination and dispersion stability hinder its application in photocatalysis [8]. Doping is an alternative solution to modify its band gap and particle size. Since TiO$_2$ [9] band gap [10] is in the UV region, its interaction with frequencies in the visible range is negligible. Hence, by shifting the absorption band [11] of TiO$_2$ towards the visible range, its photocatalytic applications [12] can be enhanced. Doping inhibits the charge recombination and improves photocatalytic activity. Doping of metal ions [13] can overcome the limitation of TiO$_2$ nanoparticles (NPs) to some extent. Several researchers have reported that doping of TiO$_2$ with specific elements, such as nitrogen (N) [14, 15], gold (Au) [16], silver (Ag) [17], platinum (Pt), palladium (Pd), copper (Cu) [18], nickel (Ni) [19] and rhodium (Rh) [20], helps in generating more electron–hole pairs and enhances the charge transfer process. Photocatalytic activity

[21, 22] has reportedly improved by addition of transition metal in TiO_2 in optimised ratio. According to reports, both nature and concentration of transition metal dopants affect the photocatalytic activity of TiO_2. Lattice structure, optical and structural properties of TiO_2 get altered by transition metal doping which depends upon the type and concentration of doped metal ion. Metal doping creates defect sites in TiO_2 [23] lattices which act as a mediator for generating free electrons and holes for photocatalytic activity. This will suppress the recombination rate of electron–hole pairs.

As reported earlier, Cr [24] doping in TiO_2 has resulted in a mixed effect on photocatalysis phenomenon. According to Li et al. [25], Cr doping increases the photocatalytic activity, whereas Herrmann [26], observed that Cr doping decreases [27] the photocatalytic action. Both the results are contradictory to each other; these results motivated us to see what exactly happens when Cr [28] doping is done in TiO_2 and how it affects the photocatalysis process. When doping concentration of 1, 5 and 10 wt % is used, unexpected blue shift due to narrowing of the band gap [11] is observed, along with the generation of new recombination centres [29], which increases the recombination rates and decreases the charge separation pair. Therefore, it is important to explore the ways in which both photocatalytic activity and recombination-related issues are addressed. Doping of Cr introduces new energy levels in the TiO_2 matrix, but an optimised concentration of dopant can improve the photocatalytic property by minimising recombination during irradiation.

In the present work, we have studied the effect of Cr doping in TiO_2 prepared by sol–gel process, photocatalytic property of pristine TiO_2 and Cr-doped TiO_2 nanoparticles. The results for both pristine and the doped nanoparticles have been compared, and the results show interesting anomalous behaviour. The study is accompanied by detailed characterisation and analysis of the pristine and Cr-doped TiO_2. We have discussed and analysed the process of suppression of photocatalysis in Cr-doped TiO_2 nanocomposite as compared to pristine TiO_2 in detail. The paper is organised as follows. In Sect. 2, we present the experimental details for preparation and characterisation of our material of interest. In Sect. 3, we discuss the experimental results and observations. Finally, in Sect. 4, we conclude the paper and compare our results with the earlier reported ones.

2 Experimental details

2.1 Material

Two precursors were used for the preparation of Cr-doped TiO_2 nanoparticles: titanium-tetra isopropoxide (TTIP) which had purity (97.8%) and chromium acetoacetate (both purchased from Sigma Aldrich). Malachite green dye (MG) and ethanoic acid of analytic grade were also acquired from Sigma Aldrich, and de-ionised (DI) water was used for preparing of aqueous solution.

2.2 Preparation Method

Sol–gel-mediated hydrothermal technique was adopted for the synthesis of pristine and Cr-doped TiO_2. 37 mL of TTIP was mixed in 250 mL of DI water with continuous stirring at low temperature which was termed as solution 1. Further, three different solutions (1, 5 and 10 wt% of chromium acetoacetate) were formed in 10 mL of DI water and termed as solution 2. Thereafter, solution 1 and solution 2 were mixed under vigorous stirring in an ice bath. The resultant solution was transferred in a water bath maintained at 80 °C and was allowed to stir until the gel was formed. Furthermore, the gel was kept at room temperature for changing the phase from solid to liquid. The resultant liquid mixture was transferred in an autoclave and put in the furnace at 220 °C for 6 h. The generated product was crushed to a fine powder after cooling at room temperature for further characterisation.

2.3 Photocatalytic Degradation: Sample preparation

During the preparation, different samples were formed for studying photocatalytic degradation of malachite green (MG) dye using pristine and Cr-doped TiO_2. For further study, the absorption coefficient of TiO_2 and MG fixed at 0.5 (arbitrary units). Afterwards, TiO_2 was added in the MG solution and kept in sunlight at intensity of 100 W/cm^2. UV absorption spectra of the resultant solution recorded after every 15 min. Photocatalytic degradation efficiency was calculated using the formula:

$$\text{Degradation Efficiency} (\%) = \left[(c_0 - c)/c_0 \right] \times 100, \qquad (1)$$

where c_0 represents initial concentration and c denotes the final concentration of the whole solution.

A similar study was carried out with Cr-doped TiO_2 and MG solution for comparison with pristine TiO_2.

2.4 Characterisation Techniques

Now, for the characterisation of the fabricated Cr-doped TiO_2 nanoparticles, Bruker-AXS D8 advanced system was used for recording the X-ray diffraction (XRD) pattern. Raman micrographs were analysed using Renishaw Invia Raman spectrophotometer, with argon laser operating at 514 nm wavelength. The Fourier transformed infrared (FTIR) spectra of the samples were recorded in the wave number range 500–5000 cm^{-1} (at a resolution of 4 cm^{-1} and averaged over 32 scans) by using FTIR spectrometer

(Nicolet 5700). Scanning electron microscope (SEM) images were obtained using Zeiss EVO MA-10 variable pressure SEM, and samples were scanned at an accelerating voltage of 10.00 kV and WD of 12.00 mm at different magnifications from 1.00 KX to 30.00 KX. For calculating the band gap of different type of nanocrystals dispersed in DI water, spectra from UV-2401 PC Shimadzu UV–Vis–NIR double-beam spectrophotometer were used. Photoluminescence (PL) spectra and charge transfer (quenching phenomenon) were measured by Horiba TCSPS model number FL-1057 PL spectrophotometer.

3 Results and Discussion

3.1 Structural characteristics

XRD is an effective characterisation which reveals whether chromium ions have been successfully doped in TiO₂ crystal lattice [30] or not. Figure 1 shows the X-ray diffraction pattern of pristine TiO₂ and Cr-doped TiO₂ nanocomposite
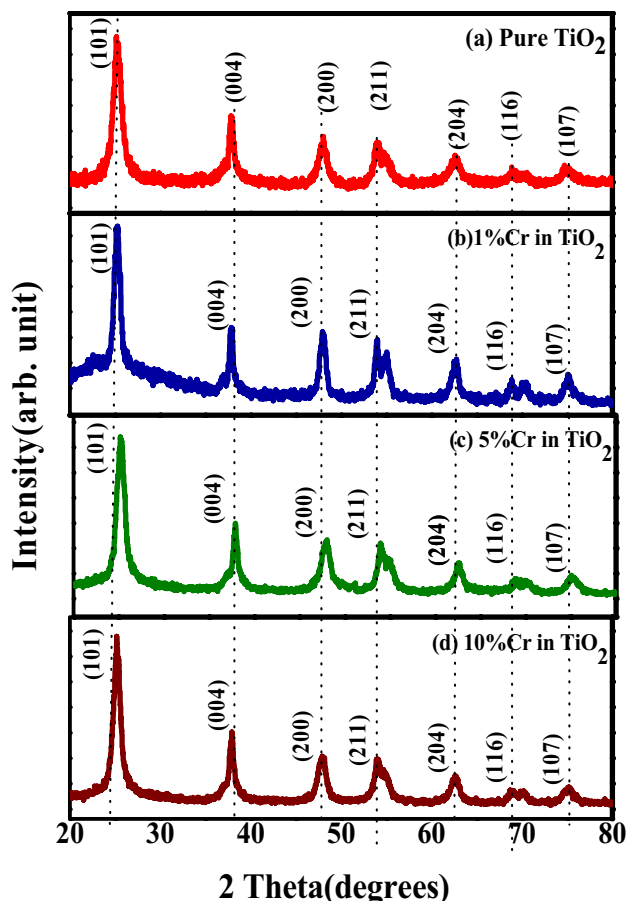

Fig. 1 XRD pattern of the pristine TiO₂ nanoparticle and Cr-doped TiO₂ nanoparticles with 0, 1, 5 and 10% concentration of Cr in TiO₂

$[Cr_{(x)}TiO_{2(1-x)}]$ with 1%, 5% and 10% by weight of Cr in TiO₂. All the samples are in anatase phase as shown in Fig. 1. The peaks at 25.3°, 37.8°, 48.0°, 55.1°, 59.5°, 65.6°, 71.2° can be ascribed to the planes (101), (004), (200), (211), (201), (116), (107) of anatase phase, respectively (JCPDS card no. 65-5714). From Fig. 1, we find that there are two twin peaks, but they are not second phase peaks in fact, they are of single anatase phase. This is also confirmed from JCPDS file. Doped Cr does not exist in any other form like Cr_2O_3 or Cr(IV) because no other phase exists in the sample. The full width half maximum (FWHM) of the XRD peaks of doped samples decreases in comparison with the pristine TiO₂ sample, indicating that Cr doping increases the crystallite size (Fig. 1). The crystallite size can be calculated using the Debye–Scherrer equation ($\tau = \frac{0.94\lambda}{\beta \cos\theta}$), where τ is the average crystallite size, λ is the wavelength of X-ray radiation, β is the FWHM, and θ is the diffraction angle, which is shown in Table 1. Ionic radius of Cr^{3+} is 62 pm and for Ti^{4+} is 60 pm which enable chromium ions to substitutionally replace titanium ions in TiO₂ lattice. It has been reported [31] that if oxidation state of dopant is less than 3+ and placed in titania lattice, it creates charge compensating anion vacancy and phase of doped titania changes from anatase to rutile, while dopant having oxidation state equal to and more than 3+ will not change the phase as also observed in this present work.

Raman analysis confirms the structural phase of pristine TiO₂ and TiO₂:Cr. It details about the local structural changes on incorporating dopant ions. Raman data, as shown in Fig. 2, affirm the results obtained from XRD data on the anatase phase of pristine TiO₂ and Cr-doped TiO₂ nanocomposite with 1, 5 and 10% by weight of Cr in TiO₂. The tetragonal anatase titania has normal vibration modes. The most active mode at 155 cm^{-1} demonstrates the well-resolved anatase phase. The peaks at 639, 516 and 397 cm^{-1} can be related to other vibration modes. There are no other peaks of oxide and Cr metal in TiO₂: Cr NPs which confirms that dopant has substitutionally interposed in the nanoparticles of TiO₂ by replacing the Ti^{4+} cations. Raman spectra verify the existence of pure anatase phase as Raman bands (235, 447 and 612 cm^{-1}) of rutile phase are absent. Raman peaks of the samples show broadness

Table 1 FWHM and grain size of Cr–TiO₂ NPs as obtained from XRD spectra

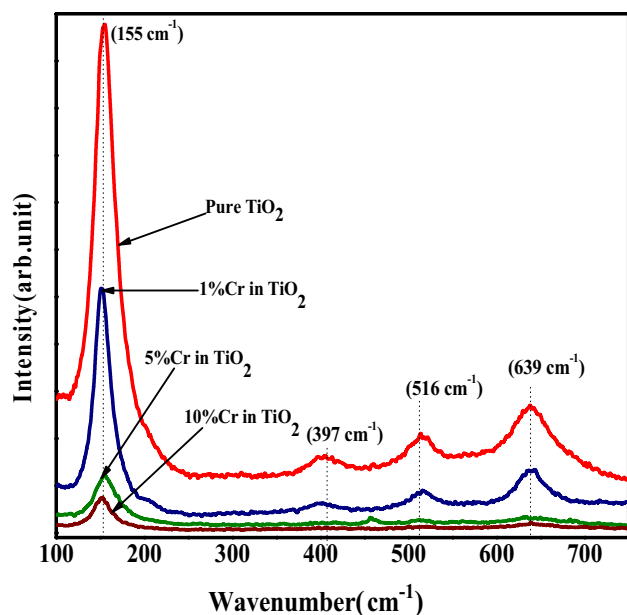| Sample (% of Cr in TiO₂)	FWHM	Crystallite size (τ)
0	0.0178	7.57 nm
1	0.0168	8.01
5	0.0174	7.75
10	0.0158	8.52

Fig. 2 Raman spectrum of the pristine TiO_2 nanoparticle and Cr-doped TiO_2 nanoparticles with 0, 1, 5 and 10% concentration of Cr in TiO_2

and significant shifting towards higher wavenumber side after varying % of chromium doping. If doping occurs on the substitutional position on the Ti^{4+} site, the Ti–O–Ti bond will get disturbed and a new Cr–O–Ti or Cr–O–Cr bond will be formed. Disturbances in the bond formation will affect the Raman-active modes and result in the broadening and shifting of the peaks. Due to the generation of the oxygen vacancies, the lattice gets contracted and the peak is shifted to a higher wavenumber. Figure 2 displays an expanded view of E_{1g} peak, and shifting increases with increasing chromium concentration. Figure 2 shows shifting in the most active vibration band position as well as changes in FWHM when the content of impurity (Cr^{3+}) is increased to a value of 5 wt %.

FTIR spectra of pristine TiO_2 and Cr-doped TiO_2 nanocomposite with 1, 5 and 10% by weight of Cr in TiO_2 are shown in Fig. 3a. The FTIR spectra exhibit peaks corresponding to the stretching vibrations of O–H that comes out to be around 3350–3450 cm^{-1}. At the same time, the bending vibrations of the adsorbed water molecules are depicted around 1620–1635 cm^{-1}. The broad and intense band between 450 and 1000 cm^{-1} is ascribed to Ti–O–Ti vibration. Previous reported works [32] mention increase in surface hydroxyl groups of TiO_2 with metal doping, which favours trapping photogenerated free radicals to enhance the charge separation efficiency. But our results suggest that as the concentration of chromium ion increases, concentration of surface hydroxyl groups decreases as shown in Fig. 3b. FTIR results validate XPS
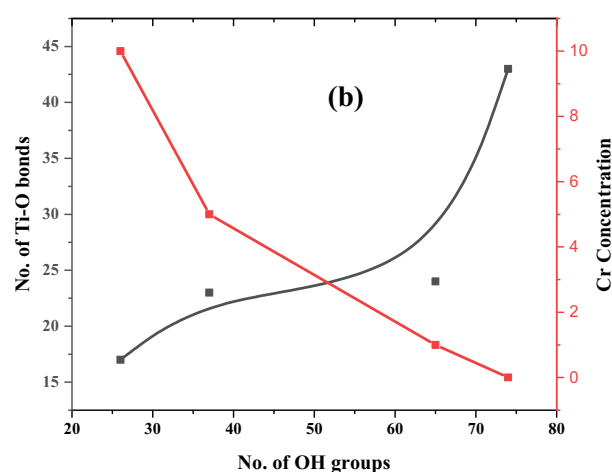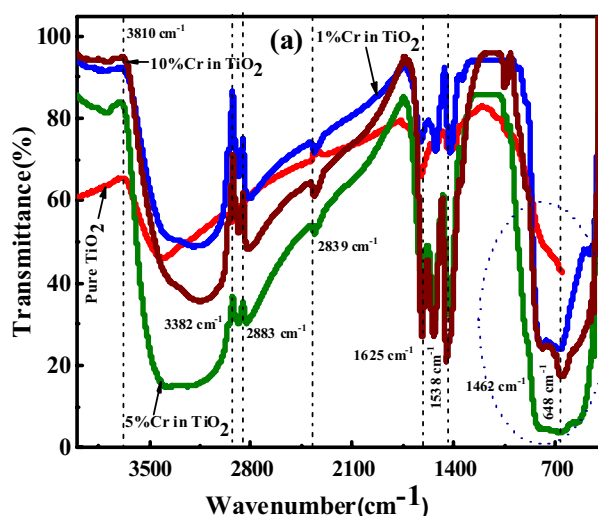

Fig. 3 **a** FTIR spectra of the pristine TiO_2 nanoparticle and Cr-doped TiO_2 nanoparticles with 0, 1, 5 and 10% concentration of Cr in TiO_2 and **b** FTIR spectra of hydroxyl group versus titanium ion of the pristine TiO_2 nanoparticle and Cr-doped TiO_2 nanopartilces with 0, 1, 5 and 10% concentration of Cr in TiO_2

results that as the chromium ion concentration increases, number of Ti^{3+} ion increases as shown in Fig. 4.

3.2 Morphological Study

The SEM micrographs of the pristine TiO_2 and $[Cr_{(x)} TiO_{2(1-x)}]$ with 1%, 5% and 10% of Cr in TiO_2 are shown in Fig. 5. From the images, the formation of spherical shaped nanoparticles with large agglomeration can be seen. It is difficult to find the particle size from the SEM images due to large agglomeration; hence, we calculate particle size from effective mass approximation method (EMA). EMA shows that as doping increases, particle size decreases which is also confirmed from Fig. 6.
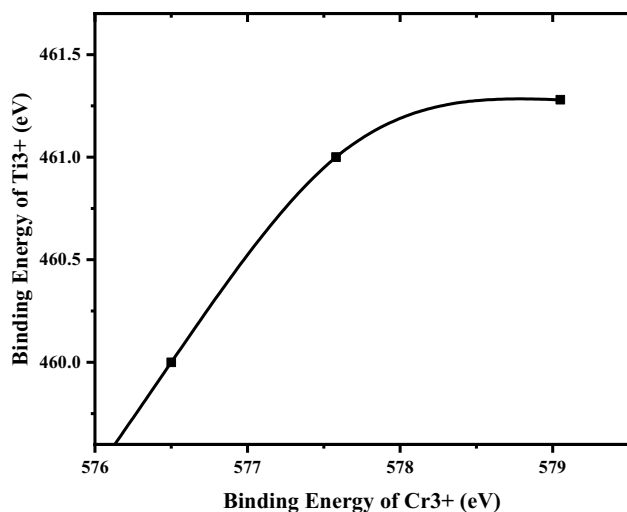
Fig. 4 XPS spectra of the pristine TiO_2 nanoparticle and Cr-doped TiO_2 nanoparticles with 0, 1, 5 and 10% concentration of Cr in TiO_2

3.3 Optical Characteristics

For optical analysis of pristine TiO_2 and $[Cr_{(x)}TiO_{2(1-x)}]$ with 0, 1, 5 and 10% of Cr in TiO_2, the variation of optical absorbance as a function of wavenumber is plotted in Fig. 6. From the plot, we observed that pristine TiO_2 absorbs only UV light with band gap 3.44 eV. This bears from the fact that the absorption spectra exhibit transition of an electron from the valence band to conduction band [33]. Absorption edge observed at 360.46, 328, 341 and 354 nm, and corresponding band gap 3.44, 3.63, 3.78 and 3.50 eV, for pristine, 1, 5, 10 wt % Cr: TiO_2, respectively. Particle size calculated by effective mass approximation shows that particle size decreases as band gap increases. Particle size is 7.03, 5.257, 4.525 and 7.31 nm for pristine, 1, 5, 10 wt % Cr:TiO_2, respectively. The band gap of pristine nanoparticles, i.e. 3.44 eV, is more than the bulk one, i.e. 3.20 eV. The reported photodegradation ratio increases with increasing the concentration of Cr metal ion in TiO_2 [34]. This indicates that the particle size is less than the Bohr diameter for TiO_2 anatase nanoparticles (2.5 nm) which shows quantum confinement effect. But in our case, observed particle size is more than the Bohr diameter; hence, no quantum confinement effect is seen which is also confirmed by Raman spectroscopy as shown in Table 2.

PL spectra of Cr-doped TiO_2 samples are obtained using xenon flash lamp having excitation wavelength of 'λex' = 250 nm as shown in Fig. 7 [35]. This is an important characterisation technique to identify the defects in the sample. Here, we have observed highly intense, polydispersed and well-resolved PL spectra of Cr-doped TiO_2. We obtained most prominent UV-emission peak within a range from 396.36 to 383.32 nm (3.12–3.25 eV), while others were less dominant [35]. The PL spectra peak at 396.36 nm results from band edge transition in the anatase phase and another peak as 383.32 is due to indirect allowed transition. Cr–TiO_2 shows change in the intensity with increase in the Cr concentration, and shifting can be easily observed. Observed blue shift at 3.12 eV cannot be attributed to quantum confinement, but is most likely due to increase in doping concentration of Cr ion creating defects since the particle size of the doped sample is more than the Bohr radius. PL fine structure can be attributed to exciton–phonon interaction [36]. Transition metal doping in nanoparticles contributes to phenomena such as band-to-band, band edge, free exciton, oxygen defect-related emission. With the doping of Cr ion in TiO_2, Ti^{4+} ion is replaced by Cr^{3+}, an oxygen vacancy is created together with reduction of Ti^{4+} ion to Ti^{3+} ion, and this oxygen vacancy is responsible for enhancing the ferromagnetic character as well as luminescence [37–39]. Number of recombination pairs increases with Cr concentration resulting in suppression of photocatalytic activity, also confirmed by TRPL results.

Time-resolved photoluminescence (TRPL) is a better analysis to study the charge recombination phenomenon. Lifetime is calculated in Fig. 8. In the case of 1 wt% Cr:T
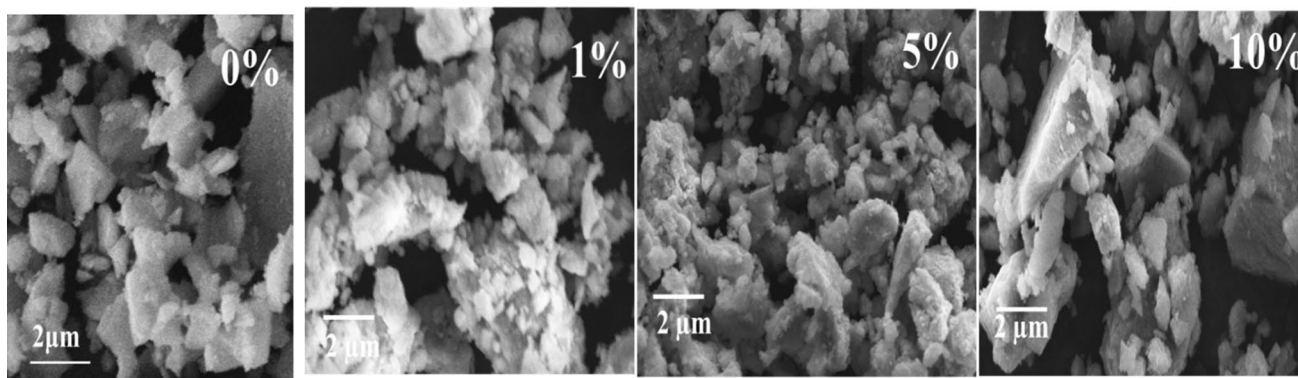

Fig. 5 Microstructure of the pristine TiO_2 nanoparticle and Cr-doped TiO_2 nanoparticles with 0, 1, 5 and 10% concentration of Cr in TiO_2
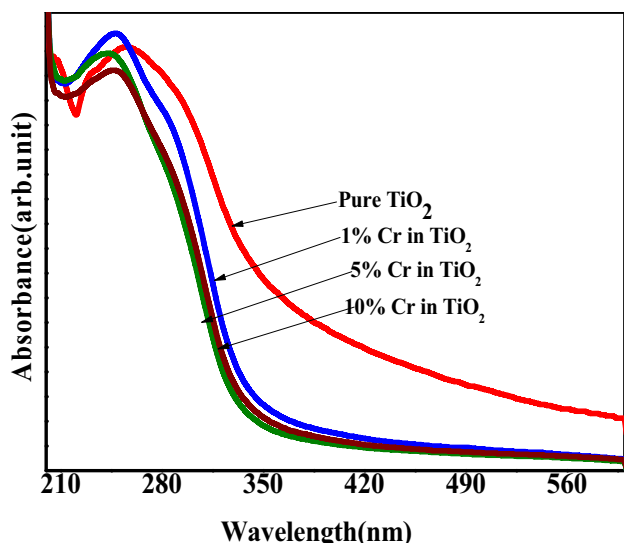
Fig. 6 UV–Vis spectra of pristine TiO$_2$ nanoparticle and Cr-doped TiO$_2$ nanoparticles with 0, 1, 5 and 10% concentration of Cr in TiO$_2$

Table 2 UV and degradation rate parameters of different Cr–TiO$_2$

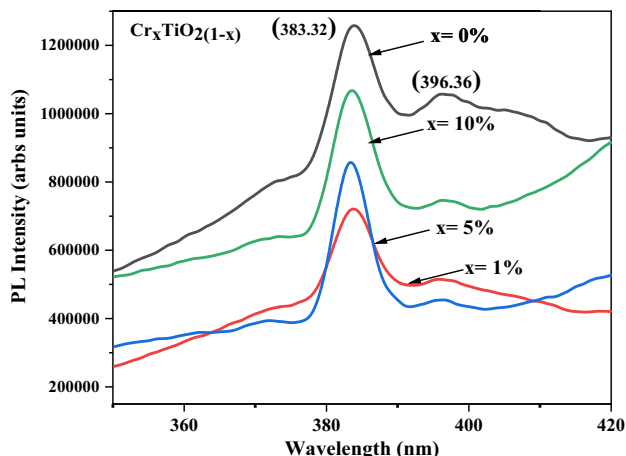| Sample (% of Cr in TiO$_2$)	Wavelength (nm)	Band gap (eV)	Degradation rate (min^{-1})
0	360.46	3.44	0.6×10^{-2}
1	341.59	3.63	1.8×10^{-2}
5	328.04	3.78	2.3×10^{-2}
10	354.28	3.50	1.5×10^{-2}

Fig. 7 PL spectra of pristine TiO$_2$ nanoparticle and Cr-doped TiO$_2$ nanoparticles with 0, 1, 5 and 10% concentration of Cr in TiO$_2$

iO$_2$, the lifetime is more than that of 10 wt% Cr: TiO$_2$. TiO$_2$ is an indirect semiconductor oxide; hence, when doping concentration of chromium increases, number of defects also increases resulting in an increase in mismatching between
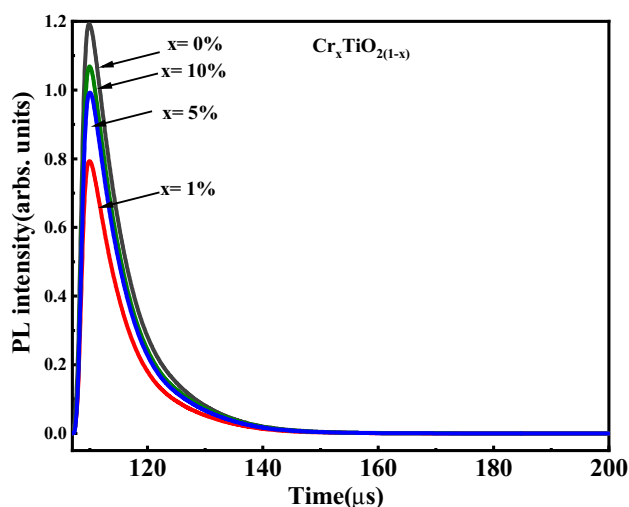
Fig. 8 TRPL spectra of pristine TiO$_2$ nanoparticle and Cr-doped TiO$_2$ nanoparticles with 0, 1, 5 and 10% concentration of Cr in TiO$_2$

Table 3 Lifetime of different Cr–TiO$_2$

Name	Lifetime (µs)
0% Cr–TiO$_2$	7.625
1% Cr–TiO$_2$	6.724
5%	6.533
10%	6.528

conduction and valence band which decreases the lifetime of charge carrier [40, 41]. A decrease in lifetime implies that the number of generated electron–hole pairs occupy/remain in the charge-trap centres (metastable state) for a shorter duration resulting in fast recombination and degradation of photocatalytic activity as shown in Table 3.

3.4 Photodegradation Dye Effect

Till now, it has been observed that with increasing Cr ion concentration, the photocatalytic activity decreases and anomalous behaviour of the Cr-doped TiO$_2$ nanoparticles is observed. Photocatalytic activity actually depends upon nanomaterial properties such as size, dispersion stability, charge separation rate and agglomeration of the nanomaterial. When agglomeration decreases, dispersion stability increases, which leads to phonon confinement of nanoparticles in nanodimensions, attributed to shift towards higher wavelength, but our results are contradictory to this study. In our case with increasing doping concentration, band gap increases, size decreases but size is more than the Bohr diameter, and hence, we rule out the phonon confinement. In Fig. 9, the absorbance spectra of MG dye, pristine TiO$_2$ nanoparticles and Cr-doped TiO$_2$ nanoparticles with 0, 1, 5 and 10% concentration of Cr in TiO$_2$ have been displayed.
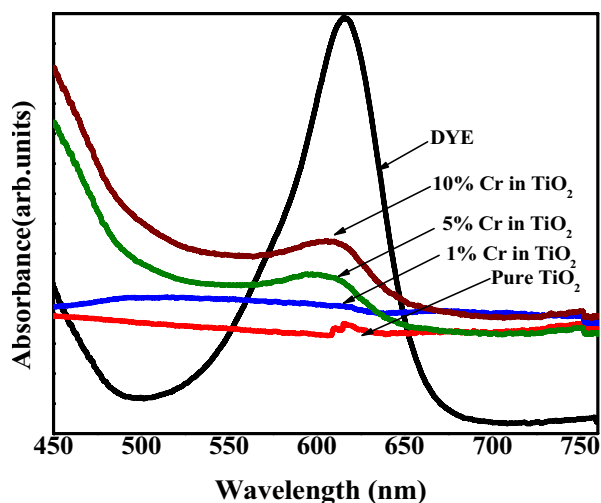
Fig. 9 Absorption spectra of MG dye, pristine TiO$_2$ nanoparticle and Cr-doped TiO$_2$ nanoparticles with 0, 1, 5 and 10% concentration of Cr in TiO$_2$

We discuss the photocatalytic behaviour of TiO$_2$ particles as a function of the wavelength of MG (an organic dye) in the presence of solar irradiation. It is found that pristine TiO$_2$ leads to rapid discolouration of the dye as compared to the Cr-doped nanoparticles for all the four concentrations of Cr in TiO$_2$. The reason behind the rapid discolouration of the dye as compared to the Cr-doped TiO$_2$ nanocomposite [42] is the breakage of Ti–O bonds which is also confirmed by Raman study. When the concentration of Cr increases, the number of available adsorption sites decreases. As a result, photocatalytic activity [43] decreases in Cr-doped TiO$_2$ nanocomposite.

3.5 The efficiency of a degraded dye

Photocatalytic decolourisation efficiency of MG dye depends on the catalyst size, catalytic activity, dispersion stability and interaction of radiation with sample. Photocatalytic degradation relies on the generation of several free radicals. The anatase phase of TiO$_2$ is recommended for higher photocatalytic activity due to the surface chemistry of dopants, and potentially high conduction band edge energy compared to doped TiO$_2$. It is also important to note that heating factor does not play any role during the time of irradiation. The reason is negligible evaporation of DI water solvent. Hence, photocatalytic activity is due to the effect of sunlight on the sample. The anatase TiO$_2$ has the drawback of higher recombination rate of OH radicals. The rate of degradation of pristine TiO$_2$ nanoparticle and Cr-doped TiO$_2$ nanocomposite with 1, 5 and 10% concentration of Cr in TiO$_2$ is shown in Fig. 10. Figure 10a shows that as the doping concentration of Cr increases,
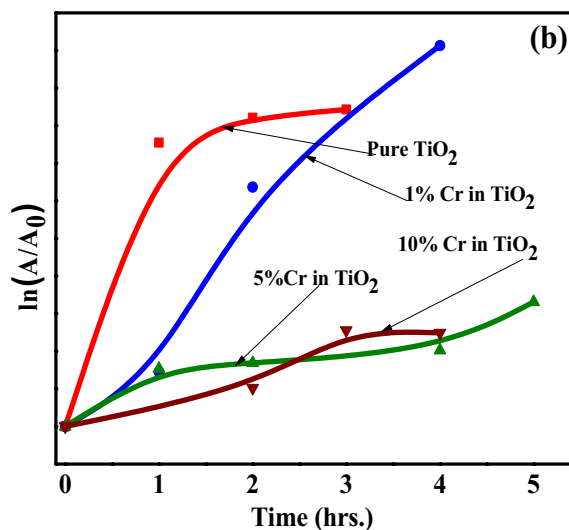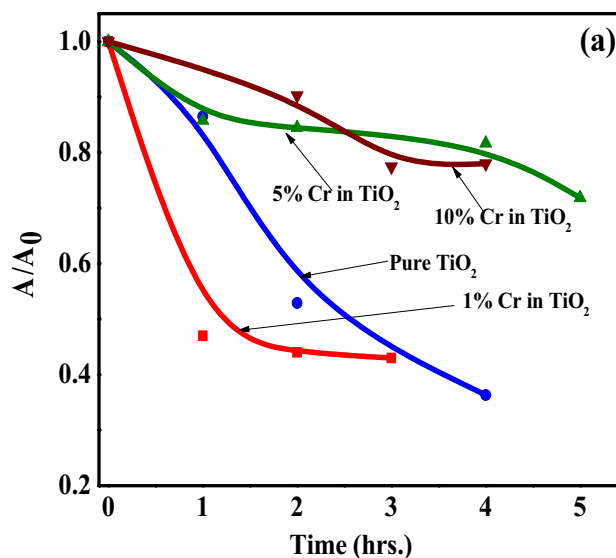

Fig. 10 a Photocatalytic degradation rate and **b** efficiency of Cr$_{(x)}$TiO$_{2(1-x)}$ with 0%, 1%, 5% and 10% of Cr with respect to MG dye

the rate of degradation decreases; this is again verified by the efficiency of degeneration given in Fig. 10b. Undoped TiO$_2$ nanoparticles show high efficiency as compared to Cr-doped TiO$_2$ nanoparticles; the reason behind this is due to the presence of oxygen vacancy. With an increase in chromium radii, oxygen vacancy also increases. In the case of 10 wt % Cr in TiO$_2$, maximum vacant sites are present which degrade photocatalytic activity. Degradation efficiency is given in Eq. 1. Efficiency for photocatalytic degradation of undoped TiO$_2$ is 96%. Degradation efficiency decreases with increased doping concentration, and for 10% Cr doping, it remains only 12%.

Photocatalytic degradation rate is given by:

$$\ln\left(\frac{C}{C_0}\right) = kt, \qquad (2)$$

where k is pseudo-first-order rate constant, and the value of k can be calculated from Fig. 10 which turns out to 0.6×10^{-2}, 1.8×10^{-2}, 2.3×10^{-2} and 1.5×10^{-2} min^{-1} for pristine, 1, 5 and 10 wt % Cr in TiO$_2$, respectively.

3.6 Degradation Mechanism

The mechanism of degradation of the MG dye can be explained by the schematic diagram shown in Fig. 9. In this figure, it is clearly shown that the energy supplied for excitation of photocatalyst free radicals, electron and hole pairs is generated by the following reaction:

$$TiO_2 + h\nu \rightarrow TiO_2 + e^-_{cb} + h^+_{vb}, \qquad (3)$$
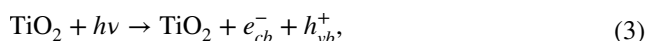
where $h\nu$ is the amount of energy required to transfer the excited electron from the valence band to the conduction band and can be equal to or greater than the band gap.

In the schematic diagram, the mechanism discussed for photocatalytic behaviour of Cr/TiO$_2$ is explained using the well known Choi's theory. According to this theory, the energy level of Cr^{3+}/Cr^{4+} lies just above the valence band of TiO$_2$, making doped Cr^{3+} acts only as a hole trapper according to the following reaction,

$$Cr^{3+} + h\nu \rightarrow Cr^{4+} + e^-_{cb}. \qquad (4)$$

Thus, the Cr/TiO$_2$ absorbed the sunlight to generate the electron–hole pairs and initiate the photocatalytic reaction. The above reaction promotes the separation of holes and electrons, thereby reducing the recombination rate. The noticeable point here is that the reaction rate can be determined by two parameters, one is how fast the electron–hole pairs are generated in the system and the other is how efficiently the charge carriers are transferred to the surface before their recombination. In our sample of interest, i.e. Cr-doped TiO$_2$ nanocomposite depicted in Fig. 11, the untrapped electron can react with the available hydrogen ions which were hydrolysed in water. At the same time, the untrapped electrons can get easily migrated to the surface and react with adsorbed O$_2$. On the other hand, the trapped holes can also be transferred to the interface and react with hydroxyl groups as shown in Eqs. (4–8). In these equations, the mechanism can be understood as follows. Reaction of Eqs. (7, 8) generates OH$^\circ$ which is an active radical possessing strong oxidising power and thus plays an important role in the overall photocatalytic reaction.
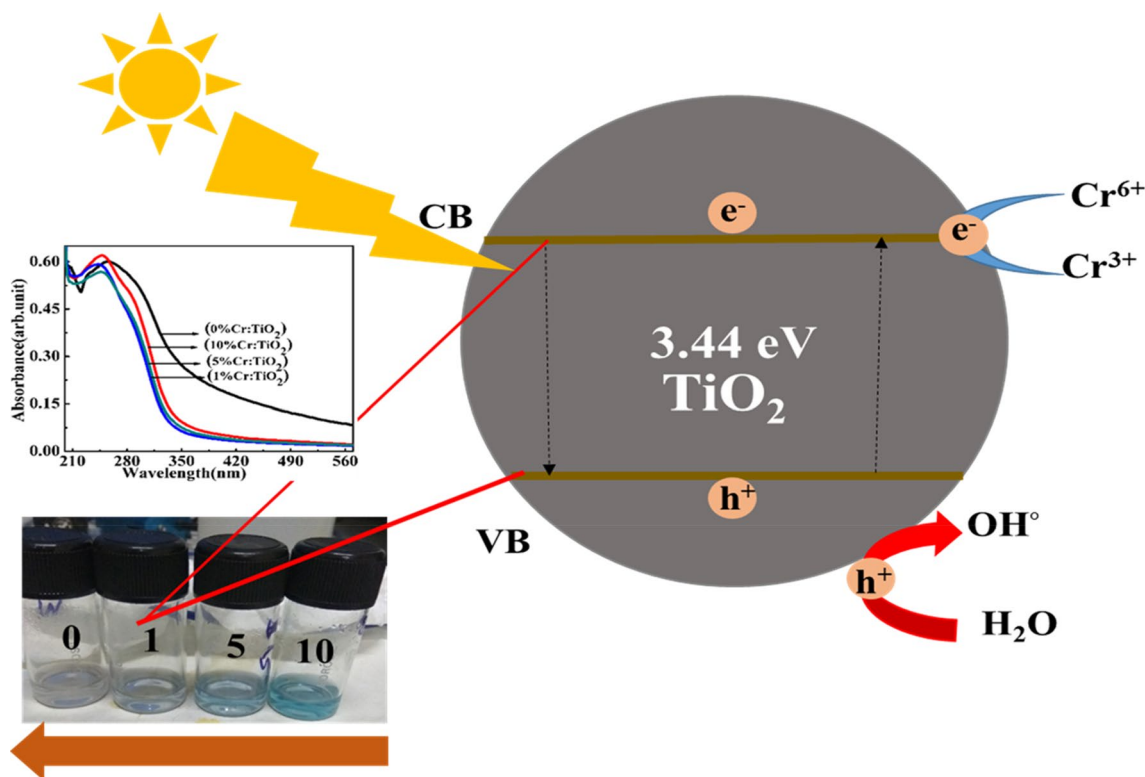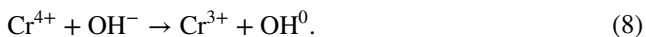

Fig. 11 Schematic diagram of [Cr$_{(x)}$TiO$_{2(1-x)}$] with 0, 1, 5 and 10% concentration of Cr in TiO$_2$ with respect to MG dye

$$2H^+ + 2e_{cb}^- \rightarrow H_2 \tag{5}$$

$$O_2 + e_{cb}^- \rightarrow O_2^- \tag{6}$$

$$O_2^- + H_2O \rightarrow OH^0 + OH^- \tag{7}$$

$$Cr^{4+} + OH^- \rightarrow Cr^{3+} + OH^0. \tag{8}$$

From the above equations, it is to note that Cr^{3+} in TiO_2 may produce over-trapping of holes with Cr^{3+}, which benefits the recombination of holes and electrons and degrade the photoactivity. In the present study, Cr-doped TiO_2 nanocomposite displays less photocatalytic activity as it possesses less adsorption sites due to increased coverage of Cr in the $Cr_xTiO_{2(1-x)}$ nanocomposite. Since doping enhances surface-to-volume ratio, sites available to the dye get enhanced. Further, in the case of acidic media, so as to increase the degradation, more electrons have to react to form oxidising species. It is a well known fact that photocatalytic activity depends upon the properties of the nanomaterial like size, surface-to-volume ratio and dispersion stability. It means that less surface adsorption sites are available for dye in Cr-doped material due to increase occupancy of $Cr_xTiO_{2(1-x)}$ by Cr. The increased incorporation of Cr^{3+} and Cr^{4+} ions in the TiO_2 matrix will screen the photocatalytic activity of Cr-doped TiO_2 as compared to undoped TiO_2.

4 Conclusion

In summary, an easy, simple and easily reproducible method has been demonstrated for the synthesis of Cr-doped TiO_2 and its photocatalytic activity on MG. The physical and chemical characterisation of nanocatalyst has been performed by XRD and FTIR which has been compared with that of standard values. Nanoanatase TiO_2 acts as a catalyst for decolouration of dye in the presence of sunlight. It has been observed that TiO_2 nanoparticles prepared by sol–gel hydrothermal route showed better photocatalytic activity as compared to Cr-doped TiO_2 nanocomposite. The increased incorporation of Cr^{3+} and Cr^{4+} ions in the TiO_2 lattice reduces the photocatalytic activity of Cr-doped TiO_2 as compared to pristine TiO_2. It has also been reported that for better photocatalytic activity lifetime increases because the number of electrons transferred from conduction band of TiO_2 to MG dye surface increases. But in our case, lifetime decreases as the concentration of Cr increases. In pristine TiO_2, we observed enhanced photocatalytic degradation as compared to doped one, which is probably due to a combined effect of (a) improved adsorption of dye on its surface (b) improved visible light absorption (c) higher lifetime of

the charge carriers and (d) narrower particle size. Along with decolourisation, 96% mineralisation of MG also achieved with pristine TiO_2 under solar irradiation. In the end, the obtained results have been compared with the reported ones.

References

1. S.H. Mohamed, M. El-Hagary, S. Althoyaib, Appl. Phys. A **111**(4), 1207 (2013)
2. N.H. Shamsudin, S. Shafie, M.Z.A. Ab Kadir, F. Ahmad, A.R. Sadrolhosseini, Y. Sulaiman, S.A.M. Chachuli, Optik **203**, 163567 (2020)
3. S. Bishnoi, N. Lohia, D. Rehani, S. Mehra, R. Datt, G. Gupta, D. Haranath, S. Sharma, Optik **203**, 164015 (2020)
4. S. Chackrabarti, R.A. Zargar, S. Joseph, M. Arora, A. Aziz, A.K. Hafiz, Optik **127**(20), 9966 (2016)
5. S. Kumar, J. Kumar, S. Narayan Sharma, S. Srivastava, Optik **178**, 411 (2019)
6. R.A. Zargar, S. Chackrabarti, S. Joseph, M.S. Khan, R. Husain, A.K. Hafiz, Optik **126**(23), 4171 (2015)
7. S.Z. Kang, Z. Xu, Y. Song, J. Mu, J. Dispersion Sci. Technol. **27**(6), 857 (2006)
8. F. Abbas, R. Bensaha, H. Taroré, Optik **180**, 361 (2019)
9. J. Bansal, S.K. Swami, A. Singh, T. Sarao, V. Dutta, A.K. Hafiz, S.N. Sharma, J. Dispers. Sci. Technol. (2019). https://doi.org/10.1080/01932691.2019.1699427
10. Y. Ishibai, T. Nishikawa, S. Miyagishi, J. Dispers. Sci. Technol. **27**(8), 1093 (2006)
11. R.A. Zargar, M.A. Bhat, I.R. Parrey, M. Arora, J. Kumar, A.K. Hafiz, Optik **127**(17), 6997 (2016)
12. K.B. Chaudhari, Y.N. Rane, D.A. Shende, N.M. Gosavi, S.R. Gosavi, Optik **193**, 163006 (2019)
13. R. Renugadevi, T. Venkatachalam, R. Narayanasamy, S. Dinesh Kirupha, Optik **127**(20), 10127 (2016)
14. Y. Chen, S. Zhang, Y. Yu, H. Wu, S. Wang, B. Zhu, W. Huang, S. Wu, J. Dispers. Sci. Technol. **29**(2), 245 (2008)
15. C. Chen, H. Bai, S.-M. Chang, C. Chang, W. Den, J. Nanoparticle Res. **9**(3), 365 (2007)
16. G.P. Patil, V.S. Bagal, S.R. Suryawanshi, D.J. Late, M.A. More, P.G. Chavan, Appl. Phys. A **122**(5), 560 (2016)
17. H. Sharma, R. Singhal, V.V. Siva Kumar, K. Asokan, Appl. Phys. A **122**(12), 1010 (2016)
18. S. Chackrabarti, R.A. Zargar, D. Ali, M. Arora, A. Aziz, A.K. Hafiz, Optik **127**(5), 2911 (2016)
19. T. Raguram, K.S. Rajni, Appl. Phys. A **125**(5), 288 (2019)
20. A. Iwan, B. Boharewicz, A. Hreniak, I. Tazbir, J. Chmielowiec, J. Mod. Opt. **61**(21), 1767 (2014)
21. H. Gao, M. Cai, Y. Liao, J. Dispers. Sci. Technol. **40**(10), 1469 (2019)
22. M.K. Singh, M.S. Mehata, Optik **193**, 163011 (2019)
23. S. Kumar, T. Vats, S.N. Sharma, J. Kumar, Optik **171**, 492 (2018)
24. Z. Xu, Y. Long, S.-Z. Kang, J. Mu, J. Dispersion Sci. Technol. **29**(8), 1150 (2008)
25. X. Li, Z. Guo, T. He, Phys. Chem. Chem. Phys. **15**(46), 20037 (2013)
26. J.-M. Herrmann, Catal. Today **53**(1), 115 (1999)

27. J.-M. Herrmann, New J. Chem. **36**(4), 883 (2012)
28. N. Bsiri, M.A. Zrir, M. Bouaicha, Optik **207**, 163888 (2020). https ://doi.org/10.1016/j.ijleo.2019.163888
29. N.C. Horti, M.D. Kamatagi, N.R. Patil, S.K. Nataraj, M.S. Sannaikar, S.R. Inamdar, Optik **194**, 163070 (2019)
30. S. Joseph, A.K. Hafiz, Optik **125**(12), 2734 (2014)
31. S. Mathew, P. Ganguly, S. Rhatigan, V. Kumaravel, C. Byrne, S.J. Hinder, J. Bartlett, M. Nolan, S.C. Pillai, Applied Sciences **8**(11), 2067 (2018)
32. J. Wang, L. Xiaonao, R. Li, P. Qiao, L. Xiao, J. Fan, Catal. Commun. **19**, 96 (2012)
33. G. Nagaraj, Raj A. Dhayal, Irudayaraj A. Albert, R.L. Josephine, Optik **179**, 889 (2019)
34. H. Attouche, S. Rahmane, S. Hettal, N. Kouidri, Optik **203**, 163985 (2020)
35. L. Kernazhitsky, V. Shymanovska, T. Gavrilko, V. Naumov, L. Fedorenko, V. Kshnyakin, J. Baran, J. Lumin. **166**, 253 (2015)
36. A. Hajjaji, K. Trabelsi, A. Atyaoui, M. Gaidi, L. Bousselmi, B. Bessais, M.A. El Khakani, Nanoscale Res. Lett. **9**, 543 (2014)
37. B. Choudhury, A. Choudhury, Mater. Chem. Phys. **132**(2–3), 1112 (2012)
38. B. Choudhury, A. Choudhury, Structural, optical and ferromagnetic properties of Cr doped TiO_2 nanoparticles. Mater. Sci. Eng., B **178**, 794–800 (2013)
39. C.C. Vidyasagar, H.B. Muralidhara, Y.A. Naik, G. Hosamani, M.S. Ilango, Energy Environ. Focus **4**(1), 54 (2015)
40. S. Paul, A. Choudhury, Appl. Nanosci. **4**(7), 839 (2013)
41. X. Li, Z. Guo, T. He, Phys. Chem. Chem. Phys.: PCCP **15**(46), 20037 (2013)
42. R.S. Dubey, S. Singh, Results in Physics **7**, 1283 (2017)
43. M. Guli, M. Deng, T. Bimenyimana, Z. Hu, Appl. Phys. A **123**(11), 675 (2017)